Reactivity of First-Row Transition Metal Monocations (Sc+, Ti+, V+, Zn+) with Methyl Fluoride: A Computational Study

ARTICLE *in* THE JOURNAL OF PHYSICAL CHEMISTRY A · FEBRUARY 2013

Impact Factor: 2.69 · DOI: 10.1021/jp400366k · Source: PubMed

6 AUTHORS, INCLUDING:

Adrián Varela-Álvarez
AstraZeneca
22 PUBLICATIONS **386** CITATIONS
SEE PROFILE

Víctor M Rayón
Universidad de Valladolid
60 PUBLICATIONS **1,113** CITATIONS
SEE PROFILE

Antonio Largo
Universidad de Valladolid
135 PUBLICATIONS **1,620** CITATIONS
SEE PROFILE

Carmen Barrientos
Universidad de Valladolid
124 PUBLICATIONS **1,359** CITATIONS
SEE PROFILE

THE JOURNAL OF PHYSICAL CHEMISTRY A

Article

pubs.acs.org/JPCA

Reactivity of First-Row Transition Metal Monocations (Sc^+, Ti^+, V^+, Zn^+) with Methyl Fluoride: A Computational Study

Pilar Redondo,[†] Adrián Varela-Álvarez,[‡] Víctor Manuel Rayón,[†] Antonio Largo,[†] José Ángel Sordo,[‡] and Carmen Barrientos*[,†]

[†]Departamento de Química Física y Química Inorgánica, Facultad de Ciencias, Universidad de Valladolid, 47008 Valladolid, Spain

[‡]Laboratorio de Química Computacional, Departamento de Química Física y Analítica, Facultad de Química, Universidad de Oviedo, 33006 Oviedo, Spain

ABSTRACT: The gas-phase reactivity of methyl fluoride with selected first-row transition metal monocations (Sc^+, Ti^+, V^+, and Zn^+) has been theoretically investigated. Our thermochemical and kinetics study shows that early transition-metal cations exhibit a much more active chemistry than the latest transition metal monocation Zn^+. The strong C−F bond in methyl fluorine can be activated by scandium, titanium, and vanadium monocations yielding the metal fluorine cation, MF^+. However, the rate efficiencies vary dramatically along the period 0.73 (Sc), 0.91 (Ti), and 0.028 (V) in agreement with the experimental observation. The kinetics results show the relative importance of the entrance and exit channels, apart from the "inner" bottleneck, to control the global rate constant of these reactions. At the mPW1K/QZVPP level our computed k_{global} (at 295 K), 1.99×10^{-9} cm^3 $molecule^{-1}$ s^{-1} (Sc^+), 1.29×10^{-9} cm^3 $molecule^{-1}$ s^{-1} (Ti^+), and 3.46×10^{-10} cm^3 $molecule^{-1}$ s^{-1} (V^+) are in good agreement with the experimental data at the same temperature. For the reaction of Zn^+ and CH_3F our predicted value for k_{outer}, at 295 K, 3.79×10^{-9} cm^3 $molecule^{-1}$ s^{-1}, is in accordance with the capture rate constant. Our study suggests that consideration of the lowest excited states for Ti^+ and V^+ is mandatory to reach agreement between calculations and experimental measurements.

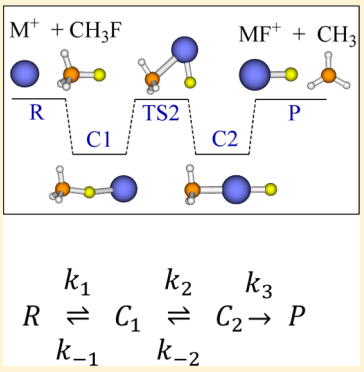

INTRODUCTION

Reactions between metal cations and organic substrates have mechanistic characteristics that are of interest from the general perspective of gas-phase chemistry[1−13] Among the organic substrates, methyl fluoride deserves a special interest. It constitutes a simple molecule to analyze the carbon−fluorine bond activation as well as the competition between C−F and C−H activation. In this context, reactions of first-row transition-metal single-charged cations with methyl fluoride become fundamental processes due to the role that bond activation reactions play in organic chemistry, biochemistry, and catalytic processes. In addition, gas-phase reactions between metal monocations and methyl fluorine also constitute relatively simple systems in which some features of the C−F activation can be theoretically studied. Another interesting topic regarding reactions involving first-row transition metal cations is the presence of different metal low-lying excited states.

Furthermore, the gas phase is the ideal environment to study these kinds of reactions under controlled conditions and without disturbing intrinsic factors such as the presence of the solvent and strong intermolecular interactions.

Over the past few years, a wealth of exhaustive experimental information on these systems has been accumulated. Basically, experimental studies are performed from three mass-spectrometric techniques: (a) ion cyclotron resonance (IRC),[14] (b) guided ion beam (GIB),[15] and (c) selected-ion flow tube (SIFT).[16,17] However, despite the enormous amount of experimental information regarding this subject, an accurate description of the reaction mechanisms has not yet been reported. In this context, theoretical computations can offer an alternative source of information. In addition, the strong interplay between theory and experimentation is very helpful in this subject.[18]

Extensive experimental and theoretical works have been performed regarding the C−F bond activation in methyl fluoride by metal cations, and here we just mention the most relevant for our purposes. The gas-phase reactivity of CH_3F with lanthanide cations (Ln^+) was examined by Cornehl et al.[19] through Fourier-transform ion cyclotron resonance mass spectrometry giving experimental evidence for a "harpoon"-like mechanism for the F atom abstraction process. This operates via an initial electron transfer from the lanthanide cations to the fluorinated substrate in the encounter complex. This mechanism was evidenced by the correlation between the second ionization energy (SIE) of the metal and the overall observed ability of the "bare" metal cations to activate the C−F bond. Room temperature reactions of atomic lanthanide monocations with CH_3F (in He at 0.35 Torr) were studied[20] in the gas phase using an inductively coupled plasma/selected-

Received: January 11, 2013
Revised: February 25, 2013
Published: February 26, 2013

   dx.doi.org/10.1021/jp400366k | J. Phys. Chem. A 2013, 117, 2932−2943

ion flow tube (ICP/SIFT) tandem mass spectrometer to measure rate coefficients and product distributions. From their systematic study, Koyanagi et al.[20] concluded that lanthanide cations react with methyl fluoride, at room temperature, predominantly by F-atom transfer, and the efficiency of this transfer correlates with the energy required to promote an electron to achieve a d^1s^1 excited electronic configuration. On the other hand, the authors exclude a direct F-atom abstraction by a "harpoon"-like mechanism on the basis of an observed noncorrelation of reaction efficiency with ionization energy (IE) of the lanthanide monocations.

More recently, the potential energy surface (PES) corresponding to the reaction of lanthanide monocations with CH_3F has been investigated using density functional theory (DFT) calculations.[21] The main conclusion in that research is that all Ln^+ reactions can be classified into one of two different reaction mechanisms, "harpoon"-like and insertion-elimination; the study shows an example of the complexity of lanthanide element chemistry.

A systematic study of the gas-phase reactions of CH_3F with a wide variety of atomic monocations using an ICP/SIFT tandem mass spectrometer operating in He at 0.35 ± 0.01 Torr and 295 ± 2 K has been carried out by Zhao et al.[22] According to the data provided by the authors, the early transition-metal cations exhibit a much more active chemistry than the late-transition-metal cations. For early transition-metal cations, fluorine atom transfer appears to be thermodynamically controlled but exhibits a periodic variation in efficiency with early transition-metal cations that maximizes with the titanium cation. Reactions including late-transition-metal cations were observed to proceed through an addition channel.

The gas-phase reactions of bare calcium monocation with organic fluorides were studied by Harvey el al.[23] using a Spectro-spin CMS 47 X FTICR mass spectrometer. In addition, the authors carried out a theoretical study employing both DFT and ab initio methodologies. From that study, the authors concluded that the reaction takes place via C−F bond activation to yield CaF^+ together with the corresponding CH_3 radical. It was also pointed out that DFT through rather popular functionals lead to underestimated reaction barriers, whereas calculations at the CCSD(T) (Coupled Cluster including single and double excitations model, augmented with a noniterative treatment of triple excitations) level with large basis sets provided a good agreement with the experiment. In addition, these authors remarked that although the theoretical exploration of the PES and the analysis in terms of the valence bond theory suggested that a "harpoon"-like mechanism seems to operate, a correlation between SIEs and reactivity does not exist. This indicates that the mechanism, through metal-mediated activation of carbon−halide bonds taking place, is not fully understood.

To confirm Harvey et al.'s conclusions,[23] we carried out a theoretical study[24] of the reaction between calcium monocation and fluoromethane. The main thrust of our study can be summarized through the following points: (a) density functional theory through appropriate density functionals such as mPW1K (modified Perdew−Wang−1-parameter method for kinetics) correctly describes the PES for this reaction and (b) the global rate constant is controlled by the relative values of the "outer" and "inner" transition states located on the PES. To complement this initial research, we have recently performed theoretical studies on the thermochemistry and kinetics of the reactions between alkali earth monocations (Mg^+, Ca^+, Sr^+, and Ba^+) and CH_3F.[25] From our study, we found that the reactions seem to proceed through a "harpoon"-like mechanism. We also pointed out the relative importance of the "outer" channel, apart from the "inner" bottleneck, to control the kinetics of these processes. We concluded that further work involving other metal cations is necessary in order to confirm the general validity of the mechanistic findings reported.

Following on from our previous studies, in this article we have focused on the reactions of first-row transition metal monocations with fluoromethane. In light of the notable differences in chemical behavior of the transition metal cation with CH_3F,[22] we have chosen four transition metal cations, namely, Sc^+, Ti^+, V^+, and Zn^+, to get insight into selectivity and chemistry of C−F bond activation of fluoromethane. Sc and Ti monocations were selected as examples for the most reactive first-row transition metal cations and Zn^+ as a representative for the less reactive ones. Finally, V^+ serves as an intermediate reactivity pattern. First, we have carried out a detailed analysis of the corresponding PESs. Then, we developed kinetics analyses within the framework of statistical theories. To the best of our knowledge, no theoretical results have been reported for any of the reactions investigated in this work.

COMPUTATIONAL METHODS

Electronic Structure Calculations. Geometries and harmonic vibrational frequencies for the minima and transition states involved in the reactions of M^+ (M = Sc, Ti, V, and Zn) with CH_3F were computed at the DFT level using the modified Perdew−Wang−1-parameter method for kinetics (mPW1K) functional.[26] Following suggestions on the role of basis sets in DFT calculations,[27] we have used Ahlrichs' triple- and quadruple-ζ basis sets (TZVPP and QZVPP).[28] Geometry optimizations were performed using a tight convergence criteria and an ultrafine grid for numerical calculations. The nature of each optimized structure (minimum or first-order saddle point) on the corresponding PES was checked performing a vibrational analysis. This computation also allowed for the evaluation of the zero point vibrational energy (ZPE) corrections. The ZPE term was included in the relative energies. For transition states, we checked that the vibrational mode associated to the imaginary frequency corresponds to the correct movement of involved atoms. In addition, the intrinsic reaction coordinate (IRC)[29,30] technique was used to explore connections between transition-state structures and adjacent minima.

For the $[TiFCH_3]^+$ system, electronic energies were refined through single-point calculations at the CCSD(T) level[31] with the TZVPP basis set.[28]

The ideal gas, rigid rotor, and harmonic oscillator approximations were considered to evaluate thermodynamic functions (ΔH, ΔS, and ΔG). A temperature of 298.15 K and a pressure of 1 atm were assumed.

Electronic structure and statistical thermodynamics calculations were performed with the Gaussian 09 program package.[32]

Kinetics Calculations. For a detailed description of the kinetics formalism used in this work, we refer the reader to our previous studies.[24,25] Here we provide a summary of the most relevant features of the model.

All the PESs for the reactions studied in this work could be represented by a scheme that includes three steps. The reactions between the transition metal monocation (M^+) and CH_3F starts through a barrierless approximation of the metal

dx.doi.org/10.1021/jp400366k | J. Phys. Chem. A 2013, 117, 2932−2943

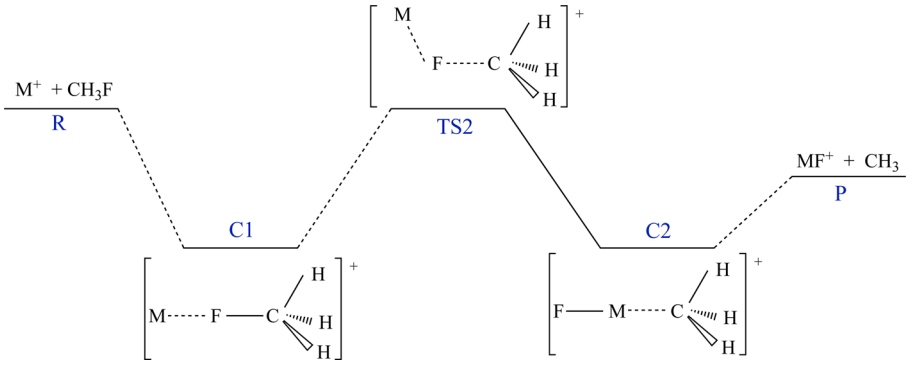

Figure 1. General representation of the potential energy surface for the $M^+ + CH_3F \rightarrow MF^+ + CH_3$ reactions (M = Sc, Ti, V, Zn).

cation to the fluorine atom of fluoromethane giving a rather stable intermediate **C1** that isomerizes into intermediate **C2** through transition structure **TS2**. Finally intermediate **C2** leads to the products through a process with no activation barrier. Figure 1 shows a simplified picture of the energy profile for the $M^+ + CH_3F$ reactions.

For kinetics calculations we have used a model developed by Mozurkewich and Benson,[33] based on the Rice−Ramsperger−Kassel−Marcus (RRKM) theory. The model was proposed for calculating rate constants of bimolecular reactions with negative activation energies and curved Arrhenius plots in apparently elementary gas-phase reactions. These reactions can be explained by assuming that an intermediate complex is formed. The rate-determining step involves a tight transition state with a rather small or negative potential energy relative to the reactants.

For both, the process of formation of initial intermediate, **C1**, and the exit channel, where no transition structures (**TS1**, **TS3**) were located, we have used the E,J-resolved microcanonical variational transition state theory (μVTST) in its vibrator formulation.[34,35] For each channel, we have constructed a distinguished-coordinate reaction path (DCP).[36,37] The points on the DCP were obtained by distinguishing one internal variable as an approximate reaction coordinate, constraining it to some predetermined value, and minimizing energy with respect to all the other internal coordinates. For these points projected-frequencies were computed.

The reaction scheme can be described by

$$R \underset{k_{-1}}{\overset{k_1}{\rightleftharpoons}} C_1 \underset{k_{-2}}{\overset{k_2}{\rightleftharpoons}} C_2 \xrightarrow{k_3} P$$

Under steady-state conditions, the rate constant for the global process can be written as

$$k_{global} = \frac{\left(\frac{2\pi\mu k_B T}{h^2}\right)^{-3/2}}{hQ_R} \sum_{J=0}^{\infty} \int_{V_{max}}^{\infty} dE\, W_1(E,J) \frac{W_2(E,J)\, W_3(E,J)}{W_2(E,J)\, W_3(E,J) + W_1(E,J)[W_2(E,J)\, W_3(E,J)]} e^{-E/RT} \quad (1)$$

Q_R represents the product of the partition functions of reactants in which the center of mass motion partition function has been factored out; V_{max} is the largest value from among the energy barriers associated to transition structures TSi (i = 1−3); and the $W_i(E,J)$ (i = 1−3) functions are the sum of states at energy lower than E and angular momentum J corresponding to the different transition structures TSi (i = 1−3) that were computed by means of the Forst algorithm.[38] T is the absolute temperature; R, k_B, and h are gas, Boltzmann, and Planck constants, and μ is the reduced mass. It should be noted that reaction symmetry factors have been included in the sums of states, $W_i(E,J)$.

As we did in our previous studies,[24,25] a two transition state model has been adopted (2-TS model). We have explicitly considered an "inner" (tighter) transition state located in the neighborhood of the first-order saddle point and an "outer" (looser) transition state controlling the entrance channel. In the case of the reaction of the zinc cation and methyl fluoride a third transition state controlling the exit channel was also considered (3-TS model).

A straightforward application of the steady-state hypothesis to the reaction scheme leads to the 3-TS $k_{global} = k_1k_2k_3/[k_2k_3 + k_{-1}(k_3 + k_{-2}]$. It reduces to the 2-TS $k_{global} = k_1k_2/(k_2 + k_{-1})$ when $k_3 \gg k_{-2}$, which is the case for all the metal ions considered in our research (except for Zn^+). In the reaction of Zn^+ with CH_3F, $k_3 \ll k_{-2}$, and thus, we have computed the global rate constant using a 3TS model.

The experimental conditions employed by Zhao et al.[22] are consistent with the main hypothesis (collisionless regime) assumed in deriving eq 1.

All the kinetics calculations were performed in the low-pressure limit by using our own routines.[24]

RESULTS AND DISCUSSION

We have investigated those electronic states arising from the ground state of the reactants. For the particular reaction of V^+ and CH_3F we have considered both triplet and quintet PESs. The triplet PES that arises from the first excited triplet state of V^+ (a^3F, $3d^34s$) was included in our study to check the possible implications of this surface through an intersystem-crossing process.

Thermochemistry. As shown in Figure 1, the first step for all reactions is the barrierless exothermic formation of an encounter complex **C1**. This arises from the direct approach of the bare monocation to the fluorine atom of fluoromethane. The interaction between both reactants is attractive because of the ion-induced dipole potential; thus, no transition structure was found on the PES. However, it is expected that an entropic bottleneck ("outer" transition state **TS1**) will appear in this region.[24,25] Once the **C1** intermediate is formed, the reaction evolves toward the formation of an insertion complex **C2** through the first order saddle point **TS2**. Finally, in the last step of the reaction, the formation of methyl radical and MF^+ takes place directly from intermediate **C2** through a barrierless

dx.doi.org/10.1021/jp400366k | J. Phys. Chem. A 2013, 117, 2932−2943

endothermic process. An entropic bottleneck should be expected in this region of the PES.

The structures of the stationary points on the PESs of the $CH_3F + M^+$ (M: Sc, Ti, V, and Zn) reactions are depicted in Figure 2, and the corresponding mPW1K/TZVPP(QZVPP) geometrical parameters are given in Table 1. As can be inferred from Table 1, the two basis sets employed in this research predict quite similar structural data.

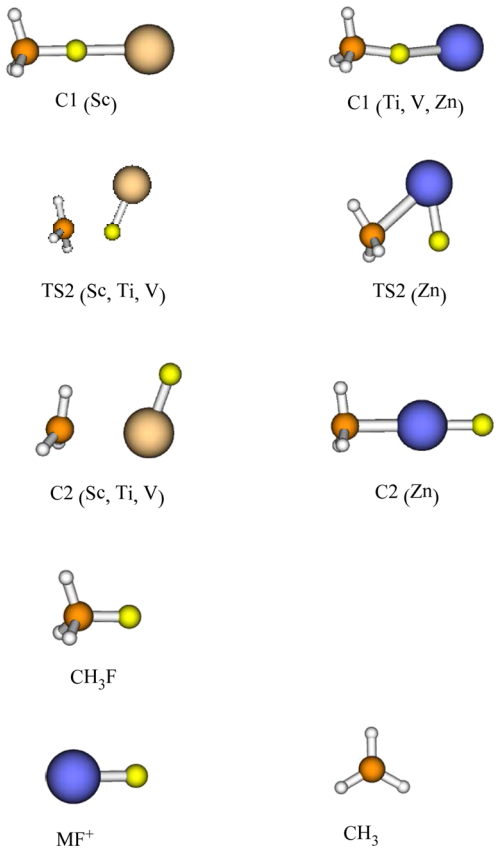

Figure 2. Structures corresponding to intermediates (C1 and C2), transition state (TS2), reactants (CH_3F), and products (MF^+ and CH_3) located on the PES.

For the reaction between the earliest transition metal monocation (Sc^+) and CH_3F, the intermediate **C1** has C_{3v} symmetry, whereas for the remaining cations this encounter complex exhibits C_S symmetry. That means that a branching point should exist along the reaction path from reactants to **C1** that displaces M^+ from the C_3 axis of CH_3F.

Regarding the transition structure geometrical parameters shown in Table 1, we find that, in all cases, the transition structure has C_1 symmetry. The M−F−C angle is clearly distorted from linearity and decreases when moving from left to right in the Periodic Table, ranging from 107.2° in Sc to 79.5 in Zn at mPW1K/QZVPP level. Except in the case of $[ZnCH_3F]^+$, the C−M bond distance is quite large; consequently, the metal will only interact with the fluorine atom. Comparing the carbon−fluorine bond length values in **C1** and **TS2**, we observe that, in all cases, this distance in **TS2** clearly enlarges in more than 0.4 Å with respect to that found in **C1**. In addition, the carbon−fluorine bond distance in **TS2** increases from Sc to Zn. These bond distance values are related to the increasing energy values of transition structure **TS2** with respect to reactants as we move from left to right along the row of the periodic table (from Sc to Zn). Finally, we observe that, in all cases, the metal−fluorine bond length in **TS2** is similar to the distance we found in isolated MF^+, suggesting a late transition state for this process.

Via transition structure **TS2**, intermediate **C1** converts to complex **C2**. Except in the reaction of Zn^+ and CH_3F, this complex has C_1 symmetry. The geometrical parameters of both methyl and metal−fluoride groups in intermediate **C2** are similar to that found in the isolated products.

Before discussing our thermochemical results, we would like to comment on the fluorine affinity data. At the mPW1K/TZVPP level the computed electronic (corrected with ZPE values) fluorine−metal affinities for the transition metal monocations selected in this work are 135.3 kcal/mol (Sc^+), 118.3 kcal/mol (Ti^+), 100.3 kcal/mol (V^+), and 56.7 kcal/mol (Zn^+). At this level of theory, the bond dissociation energy (BDE) for CH_3−F is 113.0 kcal/mol. Therefore, a priori, the formation of the fluoro metal MF^+ cannot occur in the case of zinc since at least 113 kcal/mol are required to break the CH_3−F bond whereas the energy gained in the formation of the Zn−F bond only amount to 56.7 kcal/mol.

The relative (taking the reactants as a reference) adiabatic potential energies ($\Delta U_0 = \Delta U$ + ZPE) and the Gibbs free energies (ΔG) of the intermediate species, transition structures, and products for the reactions considered in this study are detailed in Table 2. In addition, we have represented in Figure 3 a simplified picture of the energy profiles for these processes.

It should be pointed out that, for the thermal reaction of $M^+ + CH_3F$ occuring under the conditions that take place in the gas-phase experiments carried out by Zhao et al.,[22] the reactions have to be exothermic, and all intermediates and transition structures involved in the reactions must not exceed the energy of reactants.

Table 2 shows that, as it was expected, the relative energies of **C1**, **TS2**, **C2**, and products smoothly decrease when move forward in the period from scandium to zinc. This fact can be visualized in Figure 3 by the almost parallel pattern exhibited by the corresponding energy profiles for these reactions.

Analyzing intermediate **C1** energetics, we observe low bond dissociation energies of M^+−FCH_3 (ranging from 30.5 kcal/mol in Sc to 23.5 kcal/mol in Zn). This indicates a weak electrostatic interaction between M^+ and methyl fluorine.

By comparing energetics of **C1** and **C2** intermediates, it should be noted that in the reaction of early transition-metal-cations (Sc^+, Ti^+) and CH_3F, intermediate **C2** is clearly lower in energy than the encounter complex **C1** (this energy difference is in Sc^+ about 20 kcal/mol and in Ti^+ around 6 kcal/mol). This is attributable to the relatively high fluorine affinity of Sc^+ (135.3 kcal/mol at mPW1K/TZVPP level) and Ti^+·(118.3 kcal/mol at the mPW1K/TZVPP level). The energy difference between isomers **C1** and **C2** shrinks to only 2 kcal/mol in vanadium (the F atom affinity of V^+ is 100.3 kcal/mol at mPW1K/TZVPP level). Finally, the opposite is found in the reaction with zinc cation where intermediate **C2** is clearly located higher in energy than intermediate **C1** (around 25 kcal/mol) mainly due to the low fluorine affinity of Zn^+ (56.7 kcal/mol at mPW1K/TZVPP level).

Analyzing the energetic data of the transition structure, for the insertion of M^+ into the C−F bond, we observe that, in the reaction between Sc^+ and CH_3F, **TS2** is below the entrance channel (ΔU_0 = −10.4 kcal/mol, at mPW1K/QZVPP level).

For the $Ti^+ + CH_3F$ reaction the "inner" transition **TS2** state lies 2.5 kcal/mol below the reactants. It should be noted that

dx.doi.org/10.1021/jp400366k | J. Phys. Chem. A 2013, 117, 2932−2943

Table 1. Geometrical Parameters (angstroms and degrees) for the Different Species Involved in the Reaction $M^+ + CH_3F$ (M = Sc, Ti, V, Zn) at the mPW1K/TZVPP (mPW1K/QZVPP) Level of Theory

		CH_3F	C1	TS2	C2	CH_3	MF^+
$[ScCH_3F]^+$	C−H	1.085 (1.084)	1.079 (1.078)	1.079 (1.078)	1.084 (1.083)	1.074 (1.073)	-
	C−F	1.365 (1.365)	1.439 (1.438)	1.863 (1.862)	-	-	-
	C−Sc	-	-	3.024 (3.028)	2.593 (2.597)	-	-
	Sc−F	-	2.082 (2.082)	1.900 (1.900)	1.794 (1.794)	-	1.778 (1.778)
	F−C−H	109.1 (109.1)	105.9 (106.0)	108.3 (108.4)	-	-	-
	Sc−F−C	-	180.0 (180.0)	107.0 (107.2)	-	-	-
	F−Sc−C	-	-	-	109.4 (110.1)	-	-
	Sc−C−H	-	-	-	82.2 (82.3)	-	-
	H−C−Sc−F	-	0.0 (0.0)	0.0 (0.0)	0.0 (0.0)	-	-
$[TiCH_3F]^+$	C−H	1.085 (1.084)	1.079 (1.078)	1.080 (1.080)	1.083 (1.084)	1.074 (1.073)	-
	C−F	1.365 (1.365)	1.435 (1.434)	1.892 (1.890)	-	-	-
	C−Ti	-	-	2.833 (2.834)	2.508 (2.457)	-	-
	Ti−F	-	2.064 (2.064)	1.854 (1.856))	1.761 (1.736)	-	1.744 (1.747))
	F−C−H	109.1 (109.1)	106.3 (106.1)	111.9 (112.0)	-	-	-
	Ti−F−C	-	167.3 (169.9)	98.3 (98.3)	-	-	-
	F−Ti−C	-	-	41.4 (41.3)	112.5 (109.9)	-	-
	Ti−C−H	-	-	71.6 (71.6)	85.4 (84.0)	-	-
	H−C−Ti−F	-	180.0 (180.0)	180.0 (180.)	0.0 (0.0)	-	-
$[VCH_3F]^+$	C−H	1.085 (1.084)	1.080 (1.079)	1.073 (1.073)	1.082 (1.081)	1.074 (1.073)	-
	C−F	1.365 (1.365)	1.423 (1.421)	1.921 (1.919)	-	-	-
	C−V	-	-	2.675 (2.677)	2.405 (2.407)	-	-
	V−F	-	2.109 (2.115)	1.822 (1.824)	1.739 (1.741)	-	1.718 (1.721)
	F−C−H	109.1 (109.1)	107.0 (106.2)	84.6 (84.7)	-	-	-
	V−F−C	-	149.2 (150.0)	91.2 (91.3)	-	-	-
	F−V−C	-	-	-	97.48 (98.0)	-	-
	V−C−H	-	-	-	88.2 (88.1)	-	-
	H−C−V−F	-	169.7 (180.0)	180.0 (180.0)	0.0 (0.0)	-	-
$[ZnCH_3F]^+$	C−H	1.085 (1.084)	1.079 (1.078)	1.083 (1.082)	1.084 (1.084)	1.074 (1.073)	-
	C−F	1.365 (1.365)	1.440 (1.442)	2.203 (2.201)	-	-	-
	C−Zn	-		2.544 (2.563)	2.174	-	-
	Zn−F	-	2.056 (2.031)	1.779 (1.773)	1.707 (1.704)	-	1.702 (1.698)
	F−C−H	109.1 (109.1)	105.5 (106.1)	122.9 (122.2)	-	-	-
	Zn−F−C	-	159.6 (158.9)	78.6 (79.5)	-	-	-
	F−Zn−C	-	-	58.1 (57.6)	180.0 (180.0)	-	-
	Zn−C−H	-	-	79.7 (79.3)	96.5 (96.6)	-	-
	H−C−Zn−F	-	180.0 (180.0)	180.0 (179.9)	0.0 (0.0)	-	-

Table 2. mPW1K Relative (taking the reactants as a reference) Adiabatic Potential Energies ($\Delta U_0 = \Delta U$ + ZPE) and Gibbs Free Energies (ΔG) in kcal/mol As Computed at 298 K and 1 atm for the Different Species Involved in the Reaction $M^+ + CH_3F$ (M = Sc, Ti, V, Zn) in Conjunction with Ahlrichs' TZVPP and QZVPP, Second Entry, Basis Sets[a]

	$M^+ + CH_3F$		C1		TS2		C2		$MF^+ + CH_3$	
M	ΔU_0	ΔG	ΔU_0	ΔG	ΔU_0	ΔG	ΔU_0	ΔG	ΔU_0	ΔG
Sc	0.0	0.0	−30.8	−24.9	−10.6	−5.8	−50.7	−46.4	−33.9	−35.6
	0.0	0.0	−30.5	−24.7	−10.4	−5.6	−50.6	−46.3	−34.0	−35.7
Ti	0.0	0.0	−27.2	−22.8	−2.6	2.3	−37.2	−33.3	−16.8	−18.6
	0.0	0.0	−27.1	−22.7	−2.5	2.2	−32.9	−28.3	−17.0	−18.7
	(0.0)	(0.0)	(−26.4)	(−22.0)	(−3.1)	(1.9)	(−38.6)	(−34.7)	(−18.9)	(−20.6)
V (triplet PES)	0.0	0.0	−1.5	3.9	20.7	25.4	−31.6	−25.9	1.2	−0.56
	0.0	0.0	−1.4	5.0	32.3	37.7	−31.6	−25.7	0.8	−0.96
V (quintet PES)	0.0	0.0	−25.0	−20.2	6.4	11.5	−22.3	−17.9	1.2	−0.56
	0.0	0.0	−24.8	−20.2	6.4	11.5	−22.7	−18.3	0.8	−0.96
Zn	0.0	0.0	−23.0	−18.4	26.4	32.0	2.4	8.2	44.7	43.3
	0.0	0.0	−23.5	−18.5	24.4	29.8	−0.78	5.1	41.0	39.6

[a]For Ti CCSD(T)/TZVPP values are given in parentheses.

the chosen density functional, namely, mPW1K, incorrectly predicts a $3d^3$ ground state for Ti^+. This is not an unexpected result since it has been shown that most density functionals perform poorly for the calculation of s/d excitation energies[39,40] in Ti^+ yielding, in most cases, a wrong ordering of the two lowest states. The experimental ground state of Ti cation is

dx.doi.org/10.1021/jp400366k | J. Phys. Chem. A 2013, 117, 2932−2943

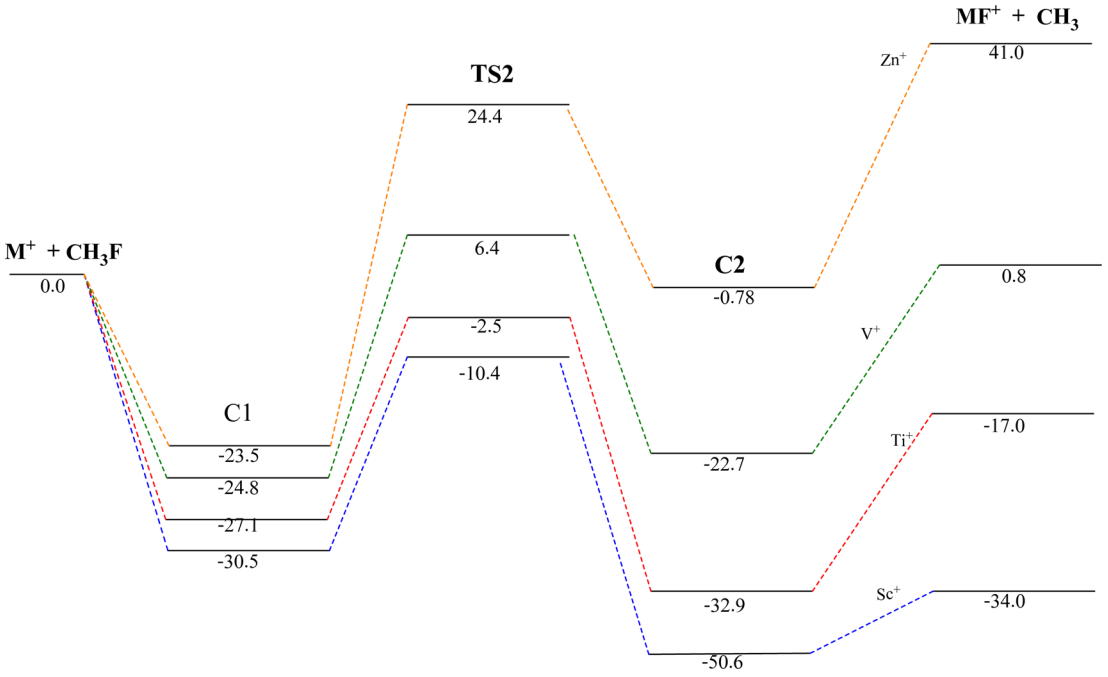

Figure 3. Energy profile for the $M^+ + CH_3F \rightarrow MF^+ + CH_3$ reactions (M = Sc, Ti, V, Zn). Values, in kcal/mol, correspond to relative (taking the reactants as a reference) adiabatic potential energies ($\Delta U_0 = \Delta U$ + ZPE) obtained at the mPW1K/QZVPP level including zero-point vibrational energy differences.

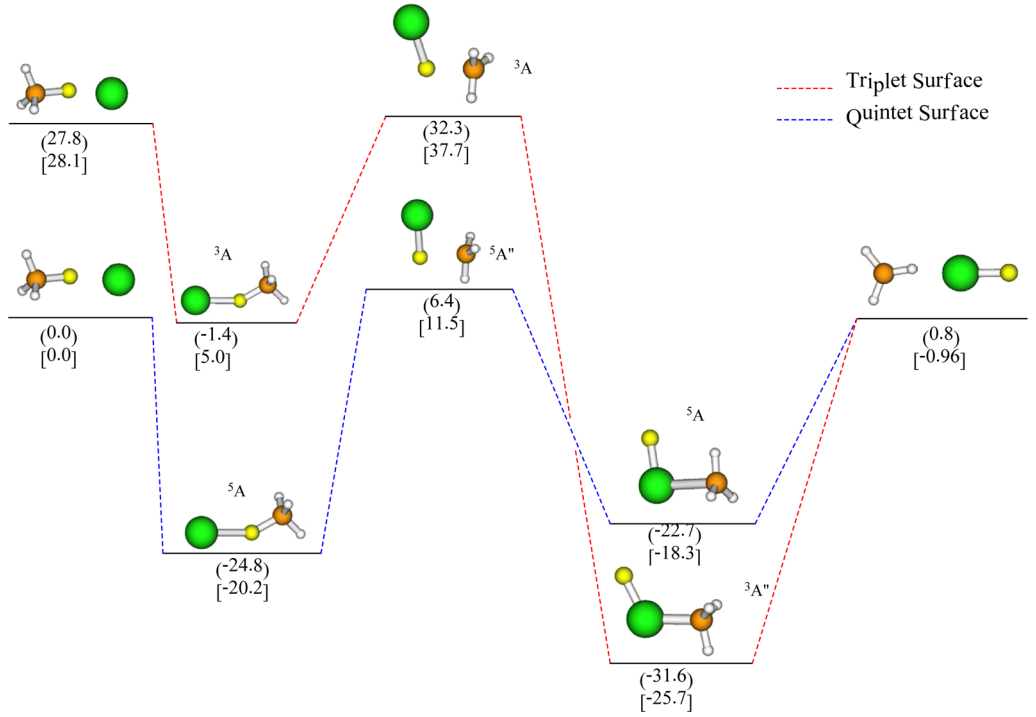

Figure 4. Energy profile (in kcal/mol) for the $V^+(^5D)/V^+(^3F) + CH_3F$ reaction at the mPW1K/QZVPP level. The relative (taking the reactants as a reference) adiabatic potential energies ($\Delta U_0 = \Delta U$ + ZPE) are given in parentheses and the Gibbs free energies in brackets [ΔG].

$4s^13d^2$ (a^4F) with the $3d^3$ (b^4F) state lying 2.5 kcal/mol higher in energy (j-averaged values).[41] The mPW1K/TZVPP level predicts $4s^13d^2$ 6.2 kcal/mol above $3d^3$ instead. We have checked that CCSD(T)/TZVPP correctly predicts $4s^13d^2$ (a^4F) below $3d^3$ (b^4F) (by 3.8 kcal/mol), and we have therefore computed the [$TiCH_3F^+$] PES at this level of theory for comparison purposes. The CCSD(T) relative energies are also presented in Table 2. In particular, we would like to draw the reader's attention to the relative energy of the "inner" transition state, **TS2**, which at this level of theory lies 3.1 kcal/mol below the reactants (Ti^+ (a^4F) + CH_3F).

For the reaction between V^+ and CH_3F, the transition structure **TS2** on the quintet PES is located above the reactants (ΔU_0 = 6.4 kcal/mol at mPW1K/QZVPP level).

In the reaction of the latest transition metal cation and CH_3F, the transition structure lies in energy clearly above the

dx.doi.org/10.1021/jp400366k | J. Phys. Chem. A 2013, 117, 2932−2943

Table 3. Kinetic Rate Coefficients in cm^3 $molecule^{-1}$ s^{-1} for the $M^+ + CH_3F$ Reactions (M = Sc, Ti, V, Zn)

	Sc^+			Ti^+			V^+			Zn^+			
T (K)	k_{outer}	k_{inner}	k_{global}	k_{outer}	k_{inner}	k_{global}	k_{outer}	k_{inner}	k_{global}	k_{outer}	k_{inner}	k_{exit}	k_{global}
135	5.30×10^{-9}	1.24×10^{-6}	3.93×10^{-9}	1.48×10^{-9}	4.57×10^{-8}	1.45×10^{-9}	2.65×10^{-8}	9.42×10^{-10}	6.76×10^{-10}	8.07×10^{-9}	1.55×10^{-51}	2.57×10^{-65}	2.56×10^{-65}
175	4.19×10^{-9}	7.74×10^{-7}	3.11×10^{-9}	1.43×10^{-9}	2.94×10^{-8}	1.35×10^{-9}	1.99×10^{-8}	6.84×10^{-10}	5.04×10^{-10}	6.00×10^{-9}	1.87×10^{-42}	1.41×10^{-52}	1.39×10^{-52}
215	3.51×10^{-9}	5.39×10^{-7}	2.58×10^{-9}	1.41×10^{-9}	2.12×10^{-8}	1.30×10^{-9}	1.62×10^{-8}	5.57×10^{-10}	4.18×10^{-10}	4.89×10^{-9}	1.02×10^{-36}	1.61×10^{-44}	1.56×10^{-44}
255	3.05×10^{-9}	4.03×10^{-7}	2.24×10^{-9}	1.40×10^{-9}	1.64×10^{-8}	1.29×10^{-9}	1.39×10^{-8}	4.90×10^{-10}	3.71×10^{-10}	4.22×10^{-9}	9.37×10^{-33}	5.97×10^{-39}	5.66×10^{-39}
295	2.74×10^{-9}	3.16×10^{-7}	1.99×10^{-9}	1.41×10^{-9}	1.33×10^{-8}	1.29×10^{-9}	1.24×10^{-8}	4.55×10^{-10}	3.46×10^{-10}	3.79×10^{-9}	7.63×10^{-30}	7.16×10^{-35}	6.62×10^{-35}
335	2.51×10^{-9}	2.56×10^{-7}	1.82×10^{-9}	1.41×10^{-9}	1.12×10^{-8}	1.30×10^{-9}	1.13×10^{-8}	4.38×10^{-10}	3.34×10^{-10}	3.49×10^{-9}	1.31×10^{-27}	9.30×10^{-32}	8.41×10^{-32}
375	2.33×10^{-9}	2.13×10^{-7}	1.69×10^{-9}	1.42×10^{-9}	9.73×10^{-9}	1.32×10^{-9}	1.05×10^{-8}	4.34×10^{-10}	3.29×10^{-10}	3.27×10^{-9}	7.75×10^{-26}	2.62×10^{-29}	2.32×10^{-29}
415	2.20×10^{-9}	1.81×10^{-7}	1.59×10^{-9}	1.42×10^{-9}	8.61×10^{-9}	1.34×10^{-9}	9.90×10^{-9}	4.38×10^{-10}	3.31×10^{-10}	3.10×10^{-9}	2.15×10^{-24}	2.46×10^{-27}	2.14×10^{-27}
455	2.09×10^{-9}	1.55×10^{-7}	1.50×10^{-9}	1.42×10^{-9}	7.74×10^{-9}	1.35×10^{-9}	9.39×10^{-9}	4.49×10^{-10}	3.36×10^{-10}	2.98×10^{-9}	3.41×10^{-23}	1.02×10^{-25}	8.79×10^{-26}
495	2.00×10^{-9}	1.35×10^{-7}	1.44×10^{-9}	1.42×10^{-9}	7.05×10^{-9}	1.37×10^{-9}	8.96×10^{-9}	4.65×10^{-10}	3.45×10^{-10}	2.87×10^{-9}	3.52×10^{-22}	2.29×10^{-24}	1.94×10^{-24}
535	1.93×10^{-9}	1.18×10^{-7}	1.39×10^{-9}	1.42×10^{-9}	6.50×10^{-9}	1.38×10^{-9}	8.60×10^{-9}	4.85×10^{-10}	3.55×10^{-10}	2.78×10^{-9}	2.60×10^{-21}	3.14×10^{-23}	2.64×10^{-23}
575	1.87×10^{-9}	1.05×10^{-7}	1.34×10^{-9}	1.42×10^{-9}	6.04×10^{-9}	1.40×10^{-9}	8.29×10^{-9}	5.08×10^{-10}	3.68×10^{-10}	2.70×10^{-9}	1.47×10^{-20}	2.94×10^{-22}	2.45×10^{-22}
615	1.81×10^{-9}	9.31×10^{-8}	1.31×10^{-9}	1.42×10^{-9}	5.66×10^{-9}	1.41×10^{-9}	8.01×10^{-9}	5.35×10^{-10}	3.82×10^{-10}	2.64×10^{-9}	6.69×10^{-20}	2.01×10^{-21}	1.66×10^{-21}
655	1.77×10^{-9}	8.33×10^{-8}	1.28×10^{-9}	1.41×10^{-9}	5.35×10^{-9}	1.42×10^{-9}	7.76×10^{-9}	5.64×10^{-10}	3.98×10^{-10}	2.58×10^{-9}	2.54×10^{-19}	1.07×10^{-20}	8.77×10^{-21}
695	1.73×10^{-9}	7.50×10^{-8}	1.25×10^{-9}	1.41×10^{-9}	5.08×10^{-9}	1.43×10^{-9}	7.54×10^{-9}	5.96×10^{-10}	4.14×10^{-10}	2.53×10^{-9}	8.26×10^{-19}	4.59×10^{-20}	3.75×10^{-20}
735	1.70×10^{-9}	6.79×10^{-8}	1.23×10^{-9}	1.40×10^{-9}	4.86×10^{-9}	1.44×10^{-9}	7.34×10^{-9}	6.30×10^{-10}	4.31×10^{-10}	2.48×10^{-9}	2.36×10^{-18}	1.65×10^{-19}	1.34×10^{-19}
775	1.67×10^{-9}	6.17×10^{-8}	1.22×10^{-9}	1.39×10^{-9}	4.67×10^{-9}	1.45×10^{-9}	7.16×10^{-9}	6.66×10^{-10}	4.49×10^{-10}	2.44×10^{-9}	6.02×10^{-18}	5.13×10^{-19}	4.15×10^{-19}
815	1.64×10^{-9}	5.63×10^{-8}	1.20×10^{-9}	1.39×10^{-9}	4.51×10^{-9}	1.46×10^{-9}	7.00×10^{-9}	7.05×10^{-10}	4.68×10^{-10}	2.40×10^{-9}	1.40×10^{-17}	1.40×10^{-18}	1.13×10^{-18}
855	1.62×10^{-9}	5.17×10^{-8}	1.19×10^{-9}	1.38×10^{-9}	4.37×10^{-9}	1.47×10^{-9}	6.85×10^{-9}	7.45×10^{-10}	4.87×10^{-10}	2.36×10^{-9}	2.97×10^{-17}	3.43×10^{-18}	2.75×10^{-18}
895	1.60×10^{-9}	4.76×10^{-8}	1.18×10^{-9}	1.38×10^{-9}	4.26×10^{-9}	1.49×10^{-9}	6.71×10^{-9}	7.87×10^{-10}	5.07×10^{-10}	2.33×10^{-9}	5.86×10^{-17}	7.64×10^{-18}	6.12×10^{-18}
935	1.59×10^{-9}	4.40×10^{-8}	1.18×10^{-9}	1.37×10^{-9}	4.16×10^{-9}	1.50×10^{-9}	6.58×10^{-9}	8.31×10^{-10}	5.27×10^{-10}	2.30×10^{-9}	1.08×10^{-16}	1.57×10^{-17}	1.25×10^{-17}
975	1.57×10^{-9}	4.09×10^{-8}	1.17×10^{-9}	1.36×10^{-9}	4.08×10^{-9}	1.51×10^{-9}	6.47×10^{-9}	8.76×10^{-10}	5.47×10^{-10}	2.27×10^{-9}	1.89×10^{-16}	2.99×10^{-17}	2.38×10^{-17}
1015	1.56×10^{-9}	3.81×10^{-8}	1.17×10^{-9}	1.36×10^{-9}	4.01×10^{-9}	1.52×10^{-9}	6.36×10^{-9}	9.22×10^{-10}	5.67×10^{-10}	2.24×10^{-9}	3.13×10^{-16}	5.35×10^{-17}	4.25×10^{-17}
1055	1.55×10^{-9}	3.56×10^{-8}	1.16×10^{-9}	1.36×10^{-9}	3.96×10^{-9}	1.54×10^{-9}	6.27×10^{-9}	9.70×10^{-10}	5.88×10^{-10}	2.22×10^{-9}	4.94×10^{-16}	9.07×10^{-17}	7.19×10^{-17}
1095	1.54×10^{-9}	3.34×10^{-8}	1.16×10^{-9}	1.35×10^{-9}	3.91×10^{-9}	1.55×10^{-9}	6.18×10^{-9}	1.02×10^{-9}	6.08×10^{-10}	2.20×10^{-9}	1.55×10^{-51}	1.46×10^{-16}	1.16×10^{-16}

dx.doi.org/10.1021/jp400366k | J. Phys. Chem. A 2013, 117, 2932−2943

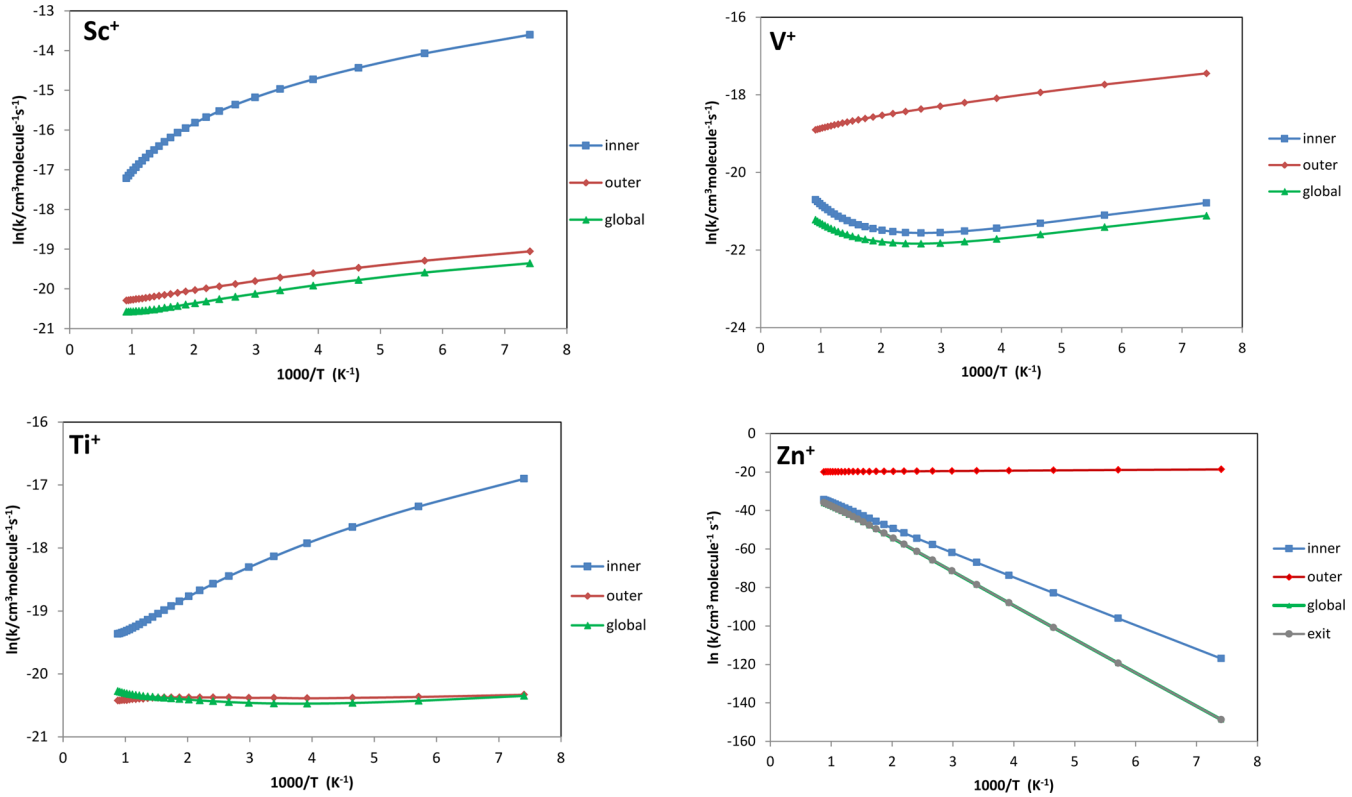

Figure 5. Arrhenius plots (k given in cm^3 molecule^{-1} s^{-1} and temperature in K) for the global rate constant, k_{global} (green), and its main limiting components: k_{inner} (blue), k_{outer}(red), and k_{exit} (gray).

reactants (ΔU_0 = 24.4 kcal/mol at mPW1K/QZVPP level) rendering thermal activation of methyl fluorine extremely improbable, consistently with the experiments.[22] Moreover, in this process the potential well associated to the encounter complex **C1** is rather deep (ΔU_0 = −23.5 kcal/mol at mPW1K/QZVPP level). This result together with the high energetic barrier found for the step **C1** → **C2** (by around 48 kcal/mol at mPW1K/QZVPP level) does explain the experimental observation of an adduct complex at room temperature.[22]

With regard energetics of the global process, we observe that, in the $Sc^+ + CH_3F$ reaction, the formation of ScF^+ is clearly exothermic and exergonic (ΔU_0 = −34.0 kcal/mol, ΔG = −35.7 kcal/mol at mPW1K/QZVPP level). We find the same behavior in the reaction between Ti^+ and CH_3F: the fluorine atom transfer process is also clearly exothermic and exergonic (ΔU_0 = −17.0 kcal/mol, ΔG = −18.7 kcal/mol at mPW1K/QZVPP level). In the reaction of V^+ (^{5}D) + CH_3F, our calculations predict an almost thermoneutral process (ΔU_0 = 0.8 kcal/mol and ΔG = −0.96 kcal/mol at mPW1K/QZVPP level). Finally the production of ZnF^+ is a clearly endothermic and endergonic process (ΔU_0 = 41.0 kcal/mol, ΔG = 39.6 kcal/mol). It should be noted that in this last reaction the transition state **TS2** and the products are clearly endothermic with respect to reactants, and thus the reaction is not expected to proceed beyond the encounter complex **C1** at least under the experimental conditions employed by Zhao et al.[22] The tendency of diminishing the exothermicity from Sc^+ to Zn^+ is again related to the decreasing affinity between fluorine and the metal when we move forward the period.

As mentioned above, for the reaction of V^+ with CH_3F we have explored both triplet and quintet surfaces in order to check if intersystem crossing might play a significant role in the reaction mechanism. The energy profile for the $V^+(^5D)/V^+(^3F)$ + CH_3F reaction is shown in Figure 4. We have identified two pathways for the formation of $VF^+(^4\Pi)$, which evolve through similar mechanisms. Overall, on both surfaces the structures of the stationary points match each other. It should be noted that the insertion-intermediate **C2** ($^3A''$) is the global minimum of both PESs. This leads to a crossing point connecting the triplet and quintet surfaces. Since this crossing point is clearly located beyond the transition structure **TS2**, along the reaction coordinate, where the elimination of VF^+ occurs, we can safely conclude that it will not alter the kinetics results.[42]

By comparing the relative adiabatic potential energies (ΔU_0 = ΔU + ZPE) and the Gibbs free energies (ΔG) data shown in Table 2, it can be inferred that the inclusion of the entropy factor results in a slight stabilization of products (by around 2 kcal/mol) and the destabilization of intermediates and transition structures (by around 5 kcal/mol) with respect to reactants.

Kinetics. The values of our calculated thermal rate constants, at several temperatures, for the four reactions studied are reported in Table 3. In Figure 5 we show the corresponding Arrhenius plots.

In order to analyze the role played by the "outer" transition state in controlling the kinetics of the reaction, we have computed the global kinetic rate constant, k_{global} (2-TS model in Sc−V and 3-TS model in Zn), as well as its limiting components, k_{inner}, k_{outer}. In the case of the Zn^+ + CH_3F reaction, the products are located clearly above both reactants and the inner transition structure, and the k_{exit} component (exit channel) has also been computed.

dx.doi.org/10.1021/jp400366k | J. Phys. Chem. A 2013, 117, 2932−2943

k_{inner} describes the limiting behavior of the global rate constant when the dominant bottleneck for the reaction is provided by the tighter "inner" transition state ($W_1(E,J) \gg W_2(E,J)$). When the looser "outer transition" state (in the entrance channel) controls the rate constant we obtain k_{outer} ($W_2(E,J) \gg W_1(E,J)$). Finally k_{exit} describes the behavior of the rate constant when the exit channel controls the process.

As stated in the Introduction, the rate coefficients for the reactions between different transition-metal monocations and fluoromethane were measured in helium at 0.35 ± 0.01 Torr and 295 ± 2 K by Zhao et al.[22] In these conditions, the observed rate constant for the reaction between Sc^+ and CH_3F is 1.1 ± 0.33 × 10^{-9} cm^3 $molecule^{-1}$ s^{-1}. As can be seen in Table 3, our computed k_{global}, at 295 K, for this process, 1.99 × 10^{-9} cm^3 $molecule^{-1}$ s^{-1}, is in reasonable agreement with the experimental value.

The Arrhenius plot for the $Sc^+ + CH_3$ reaction depicted in Figure 5 shows a similar behavior for the global rate coefficient as well as for its "inner" and "outer" components. The rate constants (k_{global}, k_{inner}, and k_{outer}) become lower as the temperature increases, a tendency found in prototypical barrierless processes.[24] In addition, since the reaction between Sc^+ and CH_3F proceeds with no activation barrier (ΔU_0 = −10.4 kcal/mol at mPW1K/QZVPP level), as expected, the global rate constant is controlled by the "outer" bottleneck in the whole range of temperatures.

As we already mentioned in the previous section, we have computed the $[TiCH_3F]^+$ PES at CCSD(T)/TZVPP level of theory for comparison purposes. At this level of theory the energy of the "inner" transition state is 3.1 kcal/mol below the reactants $Ti^+(a^4F) + CH_3F$. The relatively large experimental rate constant for this reaction (k = 1.3 ± 0.4 × 10^{-9} cm^3 $molecule^{-1}$ s^{-1})[22] suggests that, as in the case of Sc^+, the kinetics is controlled by the "outer" transition state. This fact, in turn, implies a low lying **TS2**. On the basis of our experience with this type of reaction,[24,25] this would mean that **TS2** should lie further away, 3 kcal/mol below reactants, which is not the case at the CCSD(T) level of theory. What this suggests is the involvement of an excited state of Ti^+ in this reaction. As a matter of fact, Zhao et al.[22] estimated that transition metal excited states contribute 50% or more toward the population of Ti^+. Our CCSD(T) results further suggest that involvement of the b^4F state is enough to explain the kinetic rate constant for this reaction since the "inner" transition state **TS2** lies 5.6 kcal/mol (including the a^4F−b^4F experimental gap[41]) below $Ti^+(b^4F) + CH_3F$. This barrier is fully compatible with a control exerted by an "outer" transition state as suggested by the value of the experimental rate constant. In order to compute this "outer" rate constant we would need to perform a CCSD(T) relaxed scan in the entrance channel as described in the methods section. This would be computationally prohibitive. However, Table 2 shows that the **C1** relative energy is very similar at the CCSD(T) and mPW1K levels. Therefore, we have carried out the relax scan at the mPW1K level of theory. At this level of theory, the predicted value is k_{outer} = 1.41 × 10^{-9} cm^3 $molecule^{-1}$ s^{-1} which nicely compares to the experimental (global) rate constant k = 1.3 ± 0.4 × 10^{-9} cm^3 $molecule^{-1}$ s^{-1}. We could further consider the "inner" rate constant assuming an "inner" **TS2** lying about 6 kcal/mol below reactants. This would give k_{inner} = 1.33 × 10^{-8} cm^3 $molecule^{-1}$ s^{-1} and a global rate constant (2-TS model) k = 1.29 × 10^{-9} cm^3 $molecule^{-1}$ s^{-1} which is virtually the "outer" rate constant commented above. Therefore, according to our calculations, the first excited state of Ti^+ (b^4F) does play a fundamental role in explaining the relatively large rate constant experimentally observed for the $Ti^+ + CH_3F$ reaction, in agreement with conclusions previously reported by Zhao et al.[22]

A similar conclusion is reached when analyzing our theoretical results for the reaction of V^+ and CH_3F. At mPW1K/QZVPP level of theory the "inner" transition state is 6.4 kcal/mol above the reactants $V^+(^5D) + CH_3F$. From this energy barrier, the computed rate constant, at 295 K, is 2.50 × 10^{-15} cm^3 $molecule^{-1}$ s^{-1}. The relative high value for the experimental rate coefficient (1.7 ± 0.5 × 10^{-10} cm^3 $molecule^{-1}$ s^{-1})[22] makes necessary consideration of the excited state (^5F) of vanadium monocation. Therefore, we have considered the excitation energies of V^+ (the 7.9 kcal/mol experimental s/d splitting[41]). It should be noted that in the experiments atomic ions emerge from the ICP at a nominal ion temperature of 5500 K; therefore, excited states contribute 20% or less toward the populations of Zn^+ and 50% or more toward the populations of Ti^+ with Sc^+ having intermediate distributions.[22] For the reaction of V^+ inclusion of this contribution at the mPW1K/QZVPP level lowers **TS2** 1.5 kcal/mol below reactants. Our predicted value for k_{global} at 295 K, 3.46 × 10^{-10} cm^3 $molecule^{-1}$ s^{-1}, is in agreement with the experimental (global) rate constant k = 1.7 ± 0.5 × 10^{-10} cm^3 $molecule^{-1}$ s^{-1} at that temperature. In this context, it should be pointed out that, given the accuracy achieved by the levels of theory computationally affordable nowadays, the degree of agreement between computed and experimental rate coefficients could be considered reasonable.[43] For this reaction, the transition structure **TS2** energetically lies slightly lower than reactants. At low and moderate temperatures, the "inner" rate coefficient slightly decreases as the temperature rises. From a given temperature, the entropic contribution becomes controlling, and the Arrhenius plot curves upward (see Figure 5). Thus, the Arrhenius plots exhibit a different pattern than that found in the $Sc^+/Ti^+ + CH_3F$ reactions. At 295 K, the "inner" rate constant is k_{inner} = 4.55 × 10^{-10} cm^3 $molecule^{-1}$ s^{-1} which is fully compatible with an "inner" transition rate control of the reaction.

The reaction between Zn^+ and CH_3F is clearly endothermic (ΔU_0 = 41.0 kcal/mol) and implies an important activation barrier (ΔU_0 = 24.4 kcal/mol). Thus, our calculations predict this reaction to proceed via an addition channel forming the CH_3FZn^+ adduct in agreement with the experiments.[22] For this process, we have also computed the rate coefficient for the exit channel (k_{exit}) which describes the limiting behavior of the global rate constant when the dominant bottleneck is provided by the exit channel. We observe, from Figure 5, the usual Arrhenius plot for a reaction with a net activation barrier. At low and moderate temperatures k_{global} (3-TS model) is controlled by the exit bottleneck. When the temperature rises, k_{exit} increases faster than k_{inner}. Thus, k_{inner} gives the largest contribution to k_{global} at high temperatures. As expected, in this reaction the "outer" component does not appreciably contribute to the global rate constant.

In the experiments of Zhao et al.[22] the addition reactions are expected to be termolecular with helium buffer gas atoms acting as the stabilizing third body. Thus, the experimental rate coefficient for this addition reaction (4.6 ± 1.4 × 10^{-12} cm^3 $molecule^{-1}$ s^{-1}) is an effective bimolecular constant that depends on the helium pressure. In their study, Zhao et al.[22] also provide results for the capture or collision rate coefficient

dx.doi.org/10.1021/jp400366k | J. Phys. Chem. A 2013, 117, 2932−2943

Table 4. mPW1K/QZVPP Transition-Metal, Fluorine (parentheses), and CH_3 [brackets] Partial Charges (au) and Spin Densities According to Mulliken Population Analysis (MPA)[a]

	Sc	Ti	V	Zn
Partial Charges				
C1	0.810 (−0.289) [0.479]	0.807 (−0.293) [0.486]	0.852 (−0.320) [0.468]	0.825 (−0.327) [0.502]
TS2	0.985 (−0.379) [0.395]	1.001 (−0.392) [0.391]	1.008 (−0.402) [0.394]	0.986 (−0.445) [0.459]
C2	1.248 (−0.437) [0.189]	1.211 (−0.427) [0.216]	1.263 (−0.470) [0.207]	1.154 (−0.468) [0.314]
Spin Densities				
C1	2.007 (−0.007) [0.000]	3.011 (−0.012) [0.001]	4.007 (−0.009) [0.002]	0.990 (−0.005) [0.015]
TS2	1.655 (−0.016) [0.361]	2.645 (−0.016) [0.366]	3.646 (−0.002) [0.356]	0.534 (0.089) [0.378]
C2	1.142 (−0.018) [0.876]	2.206 (−0.044) [0.838]	3.162 (−0.002) [0.840]	0.230 (0.036) [0.735]

[a]MPA values for CH_3F are −0.315 (F) and 0.008 (C).

(k_c = 2.08 × 10^{-9} cm^3 $molecule^{-1}$ s^{-1}) computed using the algorithm of the modified variational transition-state/classical trajectory theory.[44] Our predicted value for k_{outer}, 3.79 × 10^{-9} cm^3 $molecule^{-1}$ s^{-1}, at 295 K, is in good agreement with this capture rate constant.

Let us make a short comment on the efficiencies (k_{global}/k_{outer}) for the reactions considered in this study. We observe that early transition-metal cations exhibit a much more active chemistry than the late-transition-metal Zn cation. The reaction efficiency becomes a maximum for Ti^+ (reaction efficiencies, at 298 K, are 0.73, 0.91, 0.028, and 1.8 × 10^{-26} for Sc^+, Ti^+, V^+, and Zn^+, respectively) in accordance with the experimental results.[22]

Before ending, we would like to comment on the possible mechanisms of these types of reactions. From several systematic analyses on the reactions between metal monocations and fluorocarbons it was concluded that these reactions might evolve mainly through two different mechanisms: (a) single-electron transfer (SET), namely, "harpoon"-like mechanism, and (b) oxidative addition.

In our previous studies[24,25] on the C−F activation in methyl fluoride by alkaline-earth monocations, we concluded that these reactions proceed through a "harpoon"-like mechanism. If such a mechanism is operating, an inverse correlation between efficiency of reaction and SIE of the metal atom should be expected.[19,23] Consequently, the relative magnitudes of the SIEs should determine the values of the rate constants. However, from our previous study,[25] we inferred that the SIE values should correlate with the energy difference between the transition structure **TS2** and the encounter complex only when the **C1** → **TS2** step is basically a charge transfer process. We also pointed out that no correlation between the global rate constants and the SIEs should be expected if the kinetics of the reaction has non-negligible contributions from the "outer" transition state. The correlation should only exist for the rate associated with the **C1** → **TS2** step. In order to check if such a conclusion remains valid in the case of the reactions of transition-metal monocations and methyl fluorine we have computed atomic charges and spin densities of the metal, fluorine, and CH_3 fragments, for the **C1**, **C2**, and **TS2** structures by means of a Mulliken population analysis (MPA) at mPW1K/TZVPP level. These data are given in Table 4.

With regard the partial charge in each $[MFCH_3]^+$ system, we observe that, except in the case of zinc, the positive charge on the metal smoothly increases when advancing from **C1** to **C2** through **TS2** on the PES, with a parallel increase in the negative charge on the fluorine atom.

The data depicted in Table 4 show that for the intermediates **C1**, the metal unit retains the spin density of the reactant metal−monocation, namely, scandium (triplet), titanium (quadruplet), vanadium (quintet), and zinc (doublet). When moving from **C1** to **C2**, the metal spin density diminishes in one unit and, at the same time, the spin density on the CH_3 fragment in parallel raises the same amount. Therefore, a charge transfer is carried out from the metal toward the F···CH_3 fragment in the transition structure **TS2**. To conclude, our computed partial charges and spin densities are compatible with a SET "harpoon"-like mechanism:

$$M^{(n)\bullet+} + F-CH_3(\mathbf{R}) \rightarrow M^{(n)\bullet+}\cdots F-CH_3(\mathbf{C1}) \rightarrow \mathbf{TS2}$$
$$\rightarrow M^{(n-1)\bullet+}\cdots F-CH_3^{\bullet}(\mathbf{C2})$$
$$\rightarrow MF^{(n-1)\bullet+} + CH_3^{\bullet}(\mathbf{P})$$

where n represents the number of unpaired electrons of the transition metal monocation (n = 2, 3, and 4 for Sc, Ti, and V, respectively).

Since the SIE for the transition metal atoms are 295 kcal/mol (Sc), 313 kcal/mol (Ti), 338 kcal/mol (V), and 414 kcal/mol (Zn),[41] the efficiencies of the reactions should follow the order Sc > Ti > V > Zn. However, our calculations predict higher reaction efficiencies for early transition metals, finding the highest rate coefficient in the titanium reaction, in agreement with the experimental observations.[22]

On the other hand our **C1** → **TS2** energy differences (Table 2) are 20.1, 19.07, 23.3, and 47.9 kcal/mol for the reactions involving Sc^+, Ti^+, V^+, and Zn^+, respectively. Therefore we do not observe a correlation between **C1** → **TS2** energy barriers and SIEs. However, we have found a clear correlation between k_{inner} and SIEs: higher SIEs lead to lower k_{inner} values.

Summarizing, when the kinetics of the reaction has non-negligible contributions from the "outer" transition state (as in the cases of Sc and Ti) no correlation between efficiency and SIE should be expected.[25,45,46] This SIE−rate coefficient relation should only operate for the "inner" rate constant and not for the global process.

CONCLUSIONS

The reactivity of several transition-metal monocations (Sc^+, Ti^+, V^+, and Zn^+) with fluoromethane has been theoretically studied. A thermochemical analysis has been carried out using density functional theory with mPW1K[26] functional in conjunction with the TZVPP and QZVPP Ahlrichs's basis sets.[28] For the $[TiFCH_3]^+$ system single-point electronic energies were also computed at the CCSD(T) level[31] with the TZVPP basis set.[28] In addition, a kinetics study on the

dx.doi.org/10.1021/jp400366k | J. Phys. Chem. A 2013, 117, 2932−2943

framework of the conventional/variational microcanonical transition state theory has been performed.

In the $Sc^+/Ti^+ + CH_3F$ reactions, the formation of the corresponding fluorine−metal cation is clearly exothermic (ΔU_0 = −34.0/−20.0 kcal/mol at the mPW1K/QZVPP level). The production of VF^+ from the reaction between $V^+ + CH_3F$ is a nearly thermoneutral process (ΔU_0 = 0.8 kcal/mol at the mPW1K/QZVPP level). Finally, the formation of ZnF^+ is a clearly endothermic process (ΔU_0 = 41.0 kcal/mol at mPW1K/QZVPP level).

Early transition-metal cations show a much more active chemistry than the latest transition metal monocation Zn^+. The first transition metal monocations, Sc^+, Ti^+, and V^+, activate the C−F bond to give the metal fluorine cation, MF^+. However, the rate efficiencies vary dramatically along the period: 0.73 (Sc), 0.91 (Ti), and 0.028 (V) in agreement with the experimental observation.[22] For the reaction between Zn^+ and CH_3F, an addition adduct is formed.

At the mPW1K/QZVPP level, our computed k_{global} values (at 295 K) for these reactions, 1.99×10^{-9} cm^3 molecule^{-1} s^{-1} (Sc^+), 1.29×10^{-9} cm^3 molecule^{-1} s^{-1} (Ti^+), and 3.46×10^{-10} cm^3 molecule^{-1} s^{-1} (V^+), are in good agreement with the experimental data at the same temperature.[22] For the reaction of Zn^+ and CH_3F our predicted value for k_{outer}, at 295 K, was 3.79×10^{-9} cm^3 molecule^{-1} s^{-1}, in good agreement with the experimental capture rate constant.

The kinetics results emerging herein show the relative importance of the entrance and exit channels, apart from the "inner" bottleneck, to control the global rate constant of these reactions. In the reactions between Sc^+/Ti^+ and CH_3F where the formation of the MF^+ is an exothermic process and the "inner" transition state is located below the reactants, the "outer" transition state controls the global process. In the reaction between V^+ and CH_3F to yield $VF^+ + CH_3$, the "inner" channel appreciable contributes to the global rate constant. Finally, in the reaction of Zn^+ and CH_3F, the exit bottleneck addresses the kinetics, as a direct consequence of the endothermicity of the products.

In agreement with conclusions previously reported by Zhao et al.[22] our calculations suggest that consideration of the lowest exited state for Ti^+ is mandatory to reach agreement between calculations and experimental measurements. According to our study, such a conclusion must be extended to the case of the $V^+ + CH_3F$ reaction.

Theoretical evidence is given for a "harpoon"-like mechanism for the F-atom abstraction process that operates via electron transfer from the transition metal cation to the CH_3F substrate in the transition structure **TS2**. However, we do not find a correlation of the SIE with the overall observed ability of the metal−monocation to activate the C−F bond in methyl fluoride. Such a correlation should only exist for the "inner" rate constant.

AUTHOR INFORMATION

Notes

The authors declare no competing financial interest.

ACKNOWLEDGMENTS

This research has been supported by the Ministerio de Educación y Ciencia of Spain (Grant QCT2010-16864)

REFERENCES

(1) Eller, K.; Schwarz, H. *Chem. Rev.* **1991**, *91*, 1121−1177.
(2) Eller, K. *Coord. Chem. Rev.* **1993**, *126*, 93−147.
(3) Weisshaar, J. C. *Acc. Chem. Res.* **1993**, *26*, 213−219.
(4) Freiser, B. S. *Acc. Chem. Res.* **1994**, *27*, 353−360.
(5) Schröder, D.; Schwarz, H.; Shaik, S. *Struct. Bonding (Berlin)*; Springer Verlag: Berlin, 2000; Vol. *97*, p 91.
(6) Mazurek, U.; Schröder, D.; Schwarz, H. *Angew. Chem., Int. Ed.* **2002**, *41*, 2538−2541.
(7) Mazurek, U.; Koszinowski, K.; Schwarz, H. *Organometallics* **2003**, *22*, 218−225.
(8) Mazurek, U.; Schwarz, H. *Chem. Commun.* **2003**, 1321−1323.
(9) Mendez, O.; Colmenares, F. *ChemPhysChem* **2010**, *11*, 1909−1917.
(10) Uppal, J. S.; Staley, R. H. *J. Am. Chem. Soc.* **1980**, *102*, 4144−4149.
(11) Caraiman, D.; Bohme, D. K. *J. Phys. Chem. A* **2002**, *106*, 9705−9717.
(12) Lavrov, V. V.; Blagojevic, V.; Koyanagi, G. K.; Orlova, G.; Bohme, D. K. *J. Phys. Chem. A* **2004**, *108*, 5610−5624.
(13) Cheng, P.; Koyanagi, G. K.; Bohme, D. K. *J. Phys. Chem. A* **2006**, *110*, 2718−2728.
(14) Kappes, M. M.; Staley, R. H. *J. Phys. Chem.* **1981**, *85*, 942−944.
(15) Fischer, E. R.; Elkind, J. L.; Clemmer, D. E.; Georgiadis, R.; Loh, S. K.; Aristov, N.; Sunderlin, L. S.; Armentrout, P. B. *J. Chem. Phys.* **1990**, *93*, 2676−2691.
(16) Koyanagi, G. K.; Baranov, V. I.; Tanner, S. D.; Bohme, D. K. *J. Anal. At. Spectrom.* **2000**, *15*, 1207−1210.
(17) Koyanagi, G. K.; Lavrov, V.; Baranov, V. I.; Bandura, D.; Tanner, S. D.; McLaren, J. W.; Bohme, D. K. *Int. J. Mass Spectrom.* **2000**, *194*, L1−L4.
(18) Chiodo, S.; Kondakova, O.; Michelini, M. C.; Russo, N.; Sicilia, E.; Irigoras, A.; Ugalde, J. *J. Phys. Chem A* **2004**, *108*, 1069−1081.
(19) Cornehl, H. H.; Hornung, G.; Schwarz, H. *J. Am. Chem. Soc.* **1996**, *118*, 9960−9965.
(20) Koyanagi, G. K.; Zhao, X.; Blagojevic, V.; Jarvis, M. J. Y.; Bohme, D. K. *Int. J. Mass. Spectrom.* **2005**, *241*, 189−196.
(21) Matsuda, A.; Mori, H. *Chem. Phys.* **2011**, *380*, 48−53.
(22) Zhao, X.; Koyanagi, G. K.; Bohme, D. K. *J. Phys. Chem. A* **2006**, *110*, 10607−10618.
(23) Harvey, J. N.; Schröder, D.; Koch, W.; Danovich, D.; Shaik, S.; Schwarz, H. *Chem. Phys. Lett.* **1997**, *278*, 391−397.
(24) Varela-Álvarez, A.; Rayón, V. M.; Redondo, P.; Barrientos, C.; Sordo, J. A. *J. Chem. Phys.* **2009**, *124309*, 1−11.
(25) Varela-Álvarez, A.; Sordo, J. A.; Redondo, P.; Largo, A.; Barrientos, C.; Rayón, V. M. *Theor. Chem. Acc.* **2011**, *128*, 609−618.
(26) Lynch, B. J.; Fast, P. L.; Harris, M.; Truhlar, D. G. *J. Phys. Chem. A* **2000**, *104*, 4811−4815.
(27) Boese, A. D.; Martin, J. M. L.; Handy, N. C. *J. Chem. Phys.* **2003**, *119*, 3005−3014.
(28) Weigend, F.; Ahlrichs, R. *Phys. Chem. Chem. Phys.* **2005**, *7*, 3297−3305.
(29) González, C.; Schlegel, H. B. *J. Chem. Phys.* **1989**, *90*, 2154−2161.
(30) González, C.; Schlegel, H. B. *J. Phys. Chem.* **1990**, *94*, 5523−5527.
(31) Raghavachari, K.; Trucks, G. W.; Pople, J. A.; Head-Gordon, M. *Chem. Phys. Lett.* **1989**, *157*, 479−483.
(32) Frisch, M. J.; Trucks, G. W.; Schlegel, H. B.; Scuseria, G. E.; Robb, M. A.; Cheeseman, J. R.; Scalmani, G.; Barone, V.; Mennucci, B.; Petersson, G. A.; Nakatsuji, H.; Caricato, M.; Li, X.; Hratchian, H. P.; Izmaylov, A. F.; Bloino, J.; Zheng, G.; Sonnenberg, J. L.; Hada, M.; Ehara, M.; Toyota, K.; Fukuda, R.; Hasegawa, J.; Ishida, M.; Nakajima, T.; Honda, Y.; Kitao, O.; Nakai, H.; Vreven, T.; Montgomery, Jr., J. A.; Peralta, J. E.; Ogliaro, F.; Bearpark, M.; Heyd, J. J.; Brothers, E.; Kudin, K. N.; Staroverov, V. N.; Kobayashi, R.; Normand, J.; Raghavachari, K.; Rendell, A.; Burant, J. C.; Iyengar, S. S.; Tomasi, J.; Cossi, M.; Rega, N.; Millam, J. M.; Klene, M.; Knox, J. E.; Cross, J. B.; Bakken, V.; Adamo, C.; Jaramillo, J.; Gomperts, R.; Stratmann, R. E.; Yazyev, O.; Austin, A. J.; Cammi, R.; Pomelli, C.; Ochterski, J. W.; Martin, R. L.; Morokuma, K.; Zakrzewski, V. G.; Voth, G. A.; Salvador, P.;

Dannenberg, J. J.; Dapprich, S.; Daniels, A. D.; Farkas, Ö.; Foresman, J. B.; Ortiz, J. V.; Cioslowski, J.; Fox, D. J. *Gaussian 09*; Gaussian, Inc.: Wallingford CT, 2009.
(33) Mozurkewich, M.; Benson, S. W. *J. Phys. Chem.* **1984**, *88*, 6429−6435.
(34) Garret, B. C; Truhlar, D. G. *J. Chem. Phys.* **1979**, *70*, 1593−1598.
(35) Hu, X.; Hase, W. L. *J. Chem. Phys.* **1991**, *95*, 8073−8082.
(36) Villá, J.; Truhlar, D. G. *Theor. Chem. Acc.* **1997**, *97*, 317−323.
(37) Villá, J.; González-Lafont, A.; Lluch, J. M.; Corchado, J. C.; García-Espinosa, J. *J. Chem. Phys.* **1997**, *107*, 7266−7274.
(38) Forst, W.; *Theory of Unimolecular Reactions*; Academic: New York, 1973.
(39) Holthausen, M. C. *J. Comput. Chem.* **2005**, *26*, 1505−1518.
(40) Schultz, N. E.; Zhao, Y.; Truhlar, D. G. *J. Comput. Chem.* **2008**, *29*, 185−189.
(41) Kramida, A.; Ralchenko, Yu.; Reader, J.; NIST ASD Team. *NIST Atomic Spectra Database*, Version 5.0 [Online]; National Institute of Standards and Technology: Gaithersburg, MD, 2012. Available http://physics.nist.gov/asd (November 6, 2012).
(42) Varela-Álvarez, A.; Markovic, D.; Vogel, P.; Sordo, J. A. *J. Am. Chem. Soc.* **2009**, *131*, 9547−9561.
(43) Wang, Y. C.; Liu, Z. Y.; Geng, Z. Y.; Yang, X. Y.; Gao, L. G.; Chen, X. X. *J. Mol. Struct. THEOCHEM* **2006**, *765*, 27−34.
(44) Su, T.; Chesnavich, W. J. *J. Chem. Phys.* **1982**, *76*, 5183−5185.
(45) Greenwald, E. E.; North, S. W.; Georgievskii, Y.; Klippenstein, S. J. *J. Phys. Chem. A* **2005**, *109*, 6031−6044.
(46) González-Lafont, A.; Lluch, J. M. *J. Mol. Struct. THEOCHEM* **2004**, *709*, 35−43.